

## Electronic Supplementary Information

### **Solar heating catalytic formic acid dehydrogenation by graphene porous foam supported tungsten nitride nanoparticles**

Jiarong Chang<sup>a1</sup>, Tianhua Hao<sup>a1</sup>, Cuncai Lv<sup>ab\*</sup>, Maoyu Xu<sup>a</sup>, Deyi Zhang<sup>a</sup>, Linjie Gao<sup>a</sup>, Shangbo Ning<sup>a</sup>, Yaguang Li<sup>a\*</sup>, Jinhua Ye<sup>a\*</sup>

<sup>a</sup> Research Center for Solar Driven Carbon Neutrality, The College of Physics Science and Technology, Hebei University, Baoding 071002, P. R. China

<sup>b</sup> Macao Institute of Materials Science and Engineering (MIMSE), MUST-SUDA Joint Research Center for Advanced Functional Materials, Macau University of Science and Technology, Taipa, Macau SAR, 999078 China

<sup>1</sup> These authors made equal contribution to this work.

\*Corresponding authors: Cuncai Lv (cuncaiv@hbu.edu.cn), Yaguang Li (liyaguang@hbu.edu.cn), Jinhua Ye (Jinhua.YE@nims.go.jp)

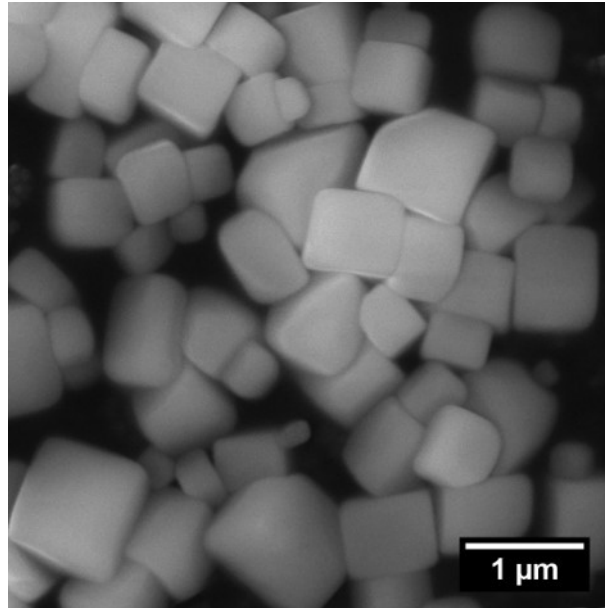


**Figure S1.** SEM image of the sample formed through freeze-drying.

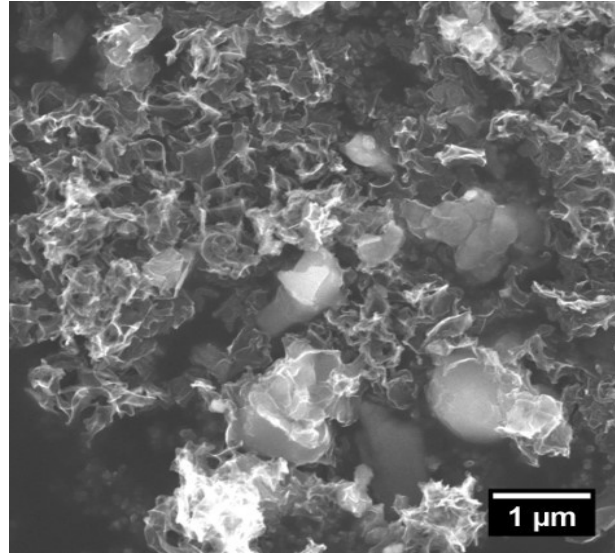


**Figure S2.** SEM image of the W/Gr PF/NaCl.

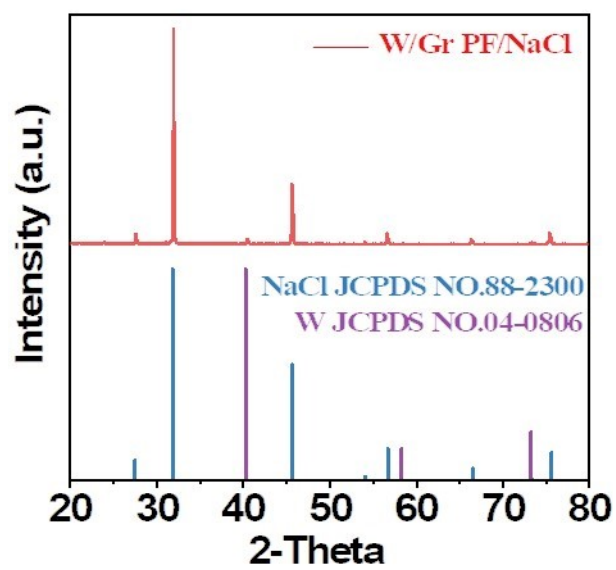


Figure S3. XRD pattern of the W/Gr PF/NaCl.

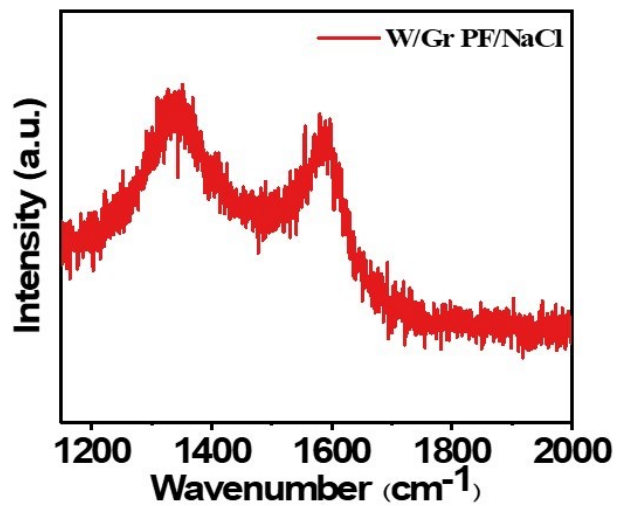
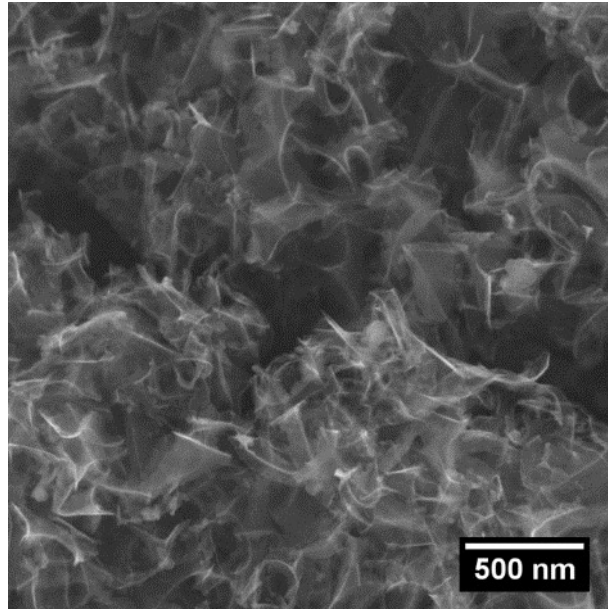
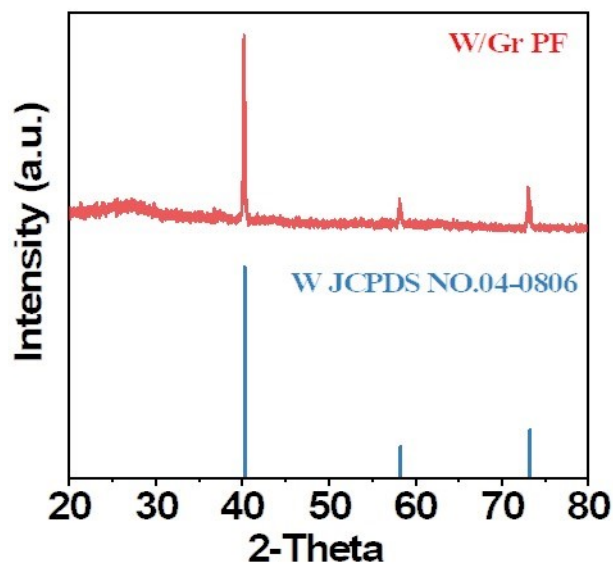


Figure S4. Raman spectrum of the W/Gr PF/NaCl.



**Figure S5.** SEM image of the W/Gr PF.



**Figure S6.** XRD pattern of the W/Gr PF.

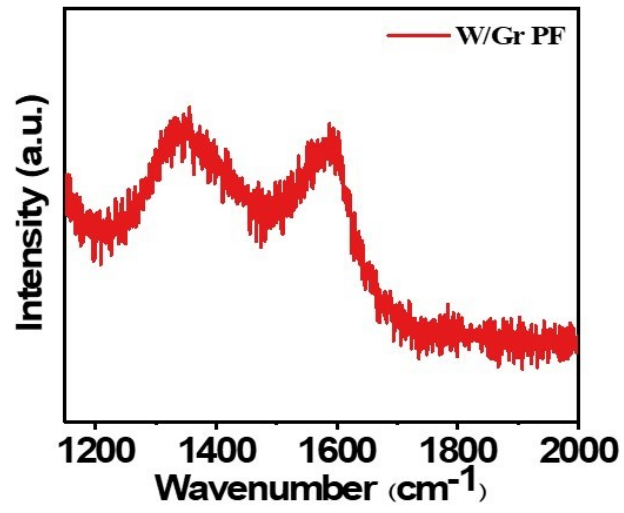


Figure S7. Raman spectrum of the W/Gr PF.



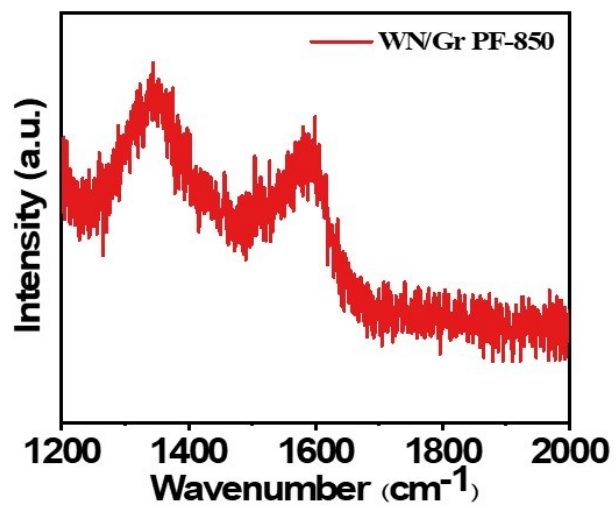
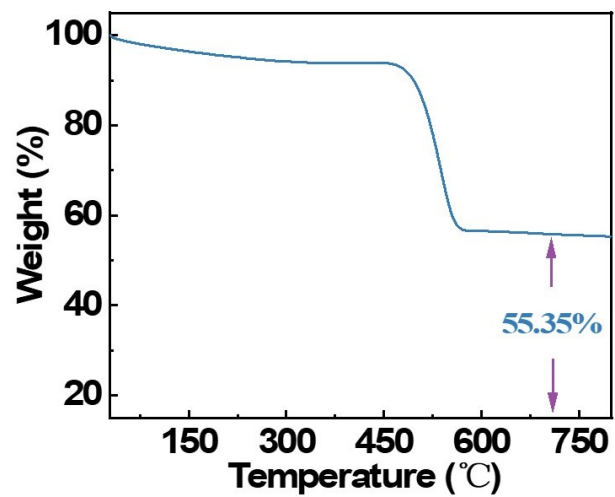
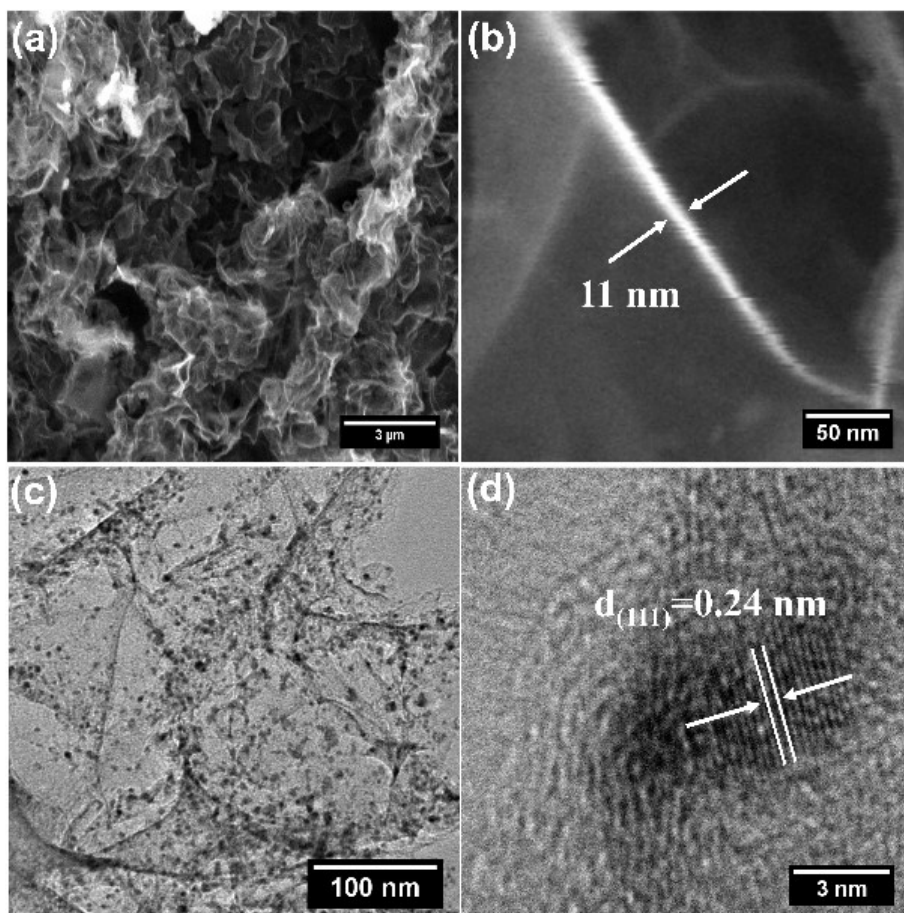


Figure S8. Raman spectrum of the WN/Gr PF-850.



**Figure S9.** The thermal gravimetric analysis (TGA) curve of WN/Gr PF-850 measured in air atmosphere.



**Figure S10.** (a, b) SEM, (c) TEM and (d) HRTEM images of WN/Gr PF-750.

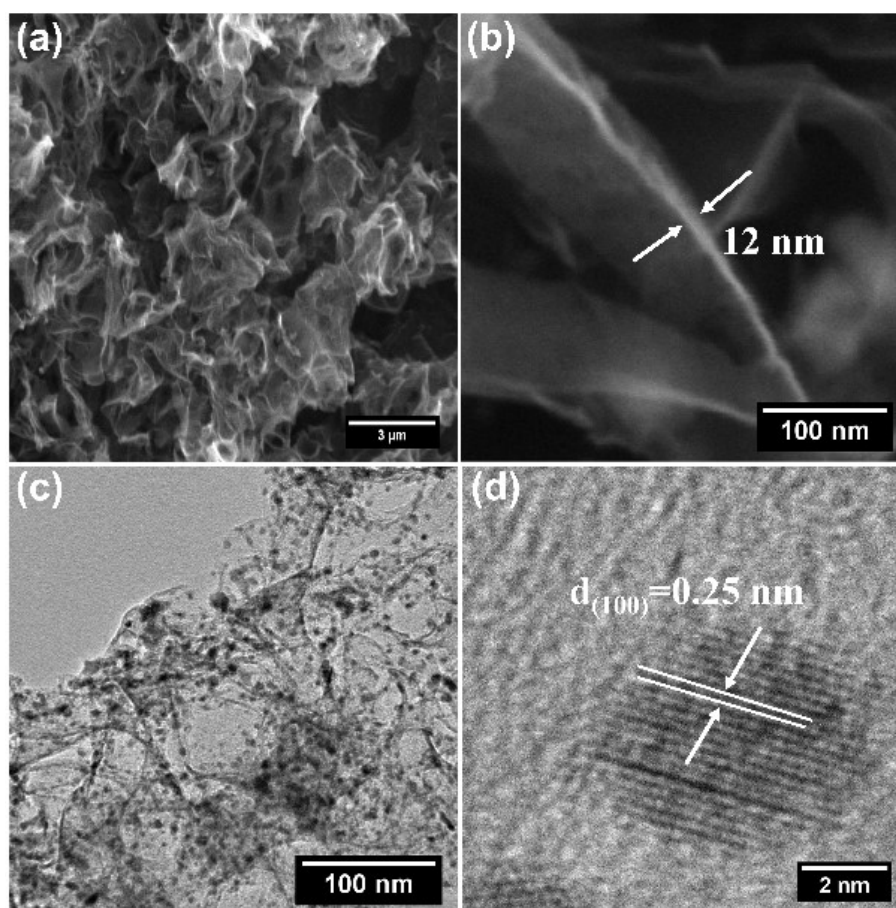


**Figure S11.** (a, b) SEM, (c) TEM and (d) HRTEM images of WN/Gr PF-950.

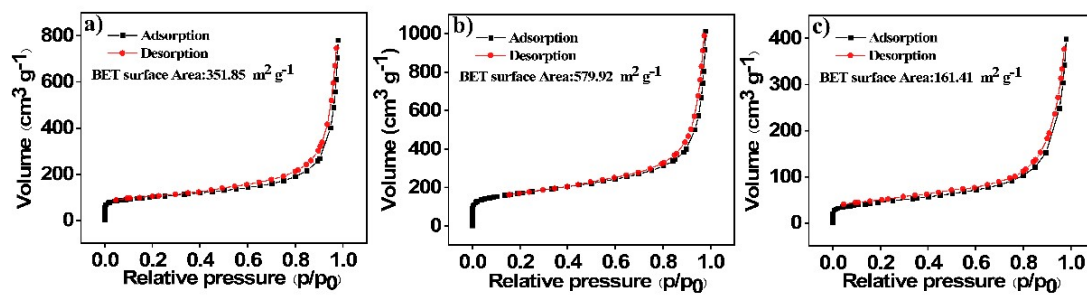
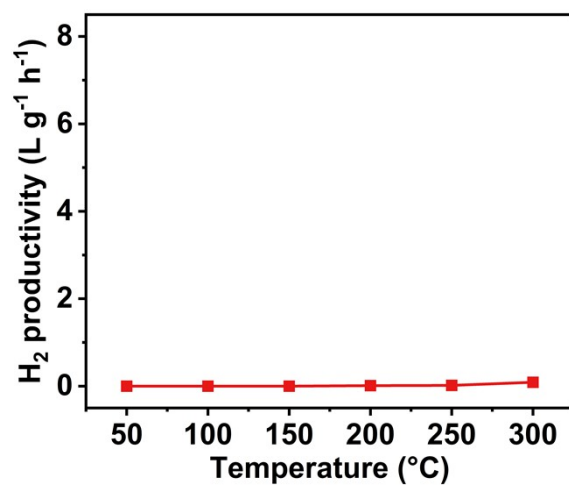
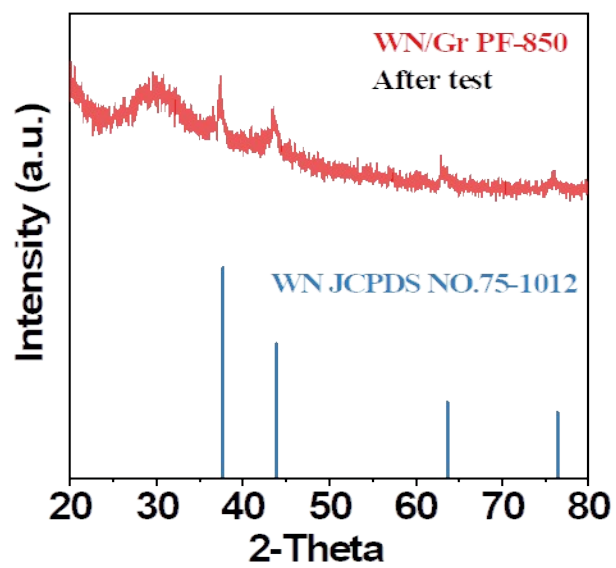


Figure S12. BET of the WN/Gr PF-750 (a), WN/Gr PF-850 (b) and WN/Gr PF-950

(c).



**Figure S13.** Thermal catalytic FA decomposition test without any catalysts.



**Figure S14.** XRD spectrum of the WN/Gr PF-850 after test.

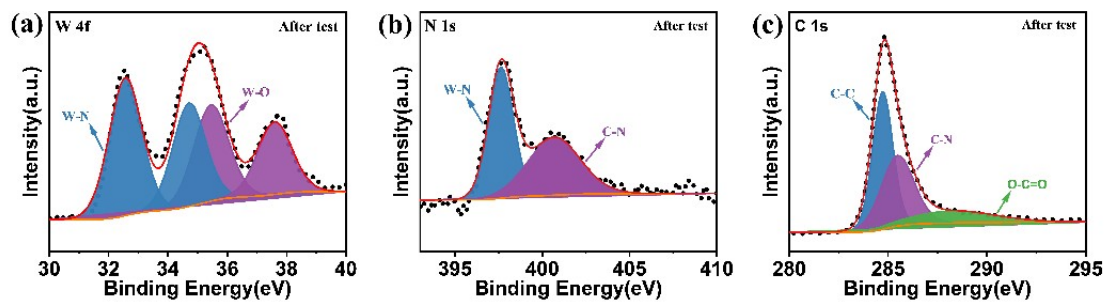


Figure S15. XPS of the WN/Gr PF-850 after test.



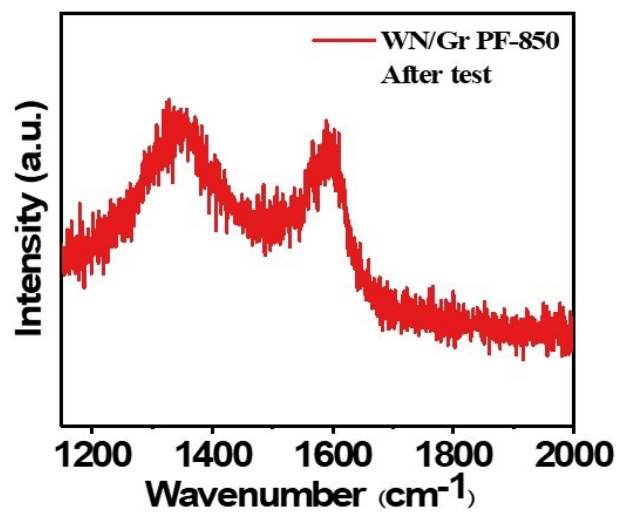
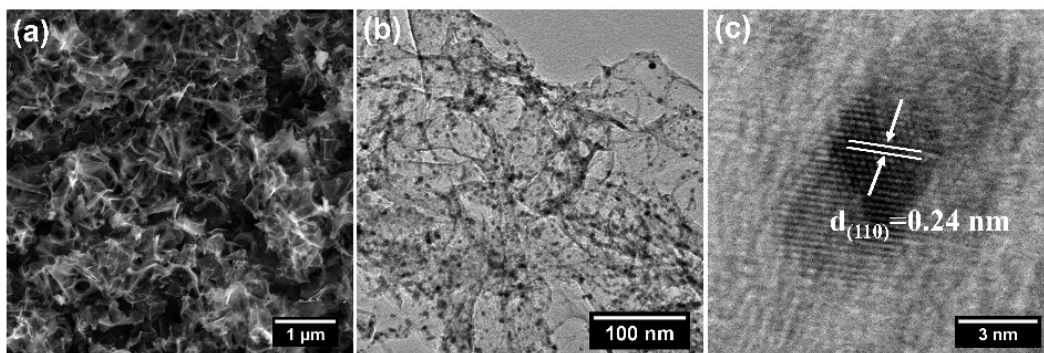
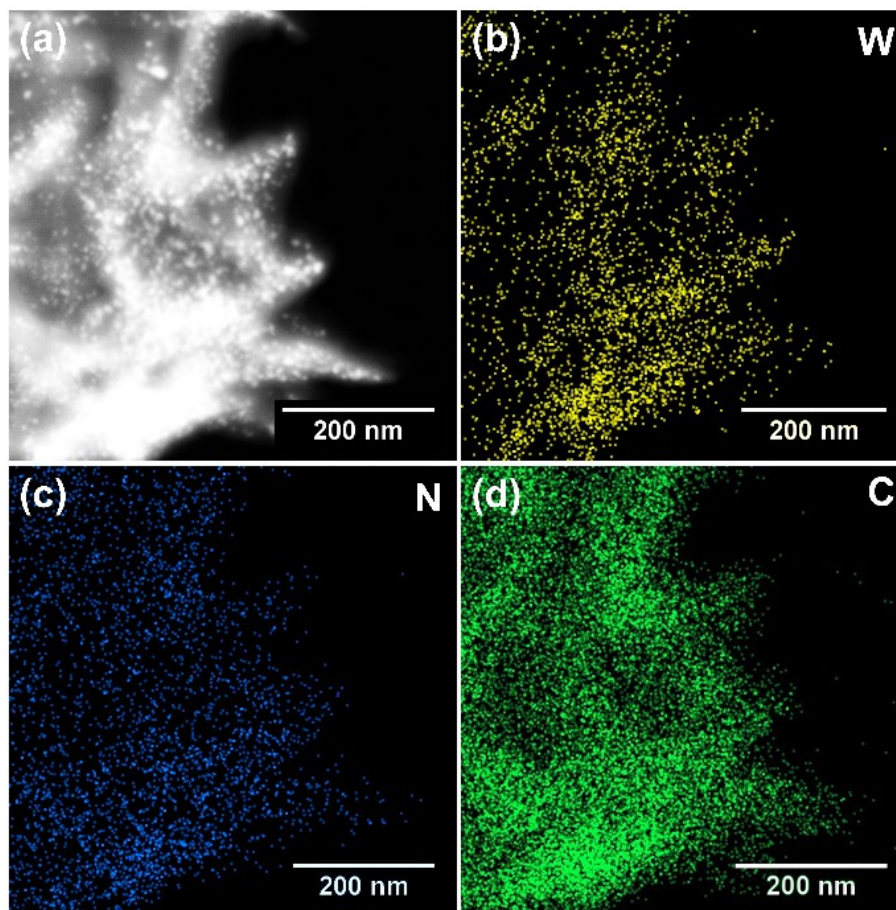


Figure S16. Raman spectrum of the WN/Gr PF-850 after test.



**Figure S17.** (a) SEM, (b) TEM, and (c) HRTEM images of WN/Gr PF-850 after test.



**Figure S18.** STEM image (a) and corresponding elemental mapping images of (a) W, (c) O and (d) C of WN/Gr PF-850 after test.

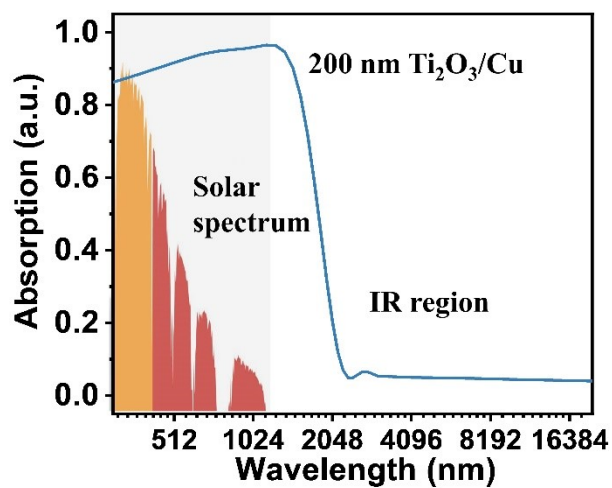


**Figure S19.** Normalized light absorption spectra of  $\text{Ti}_2\text{O}_3$  film/Cu layer.

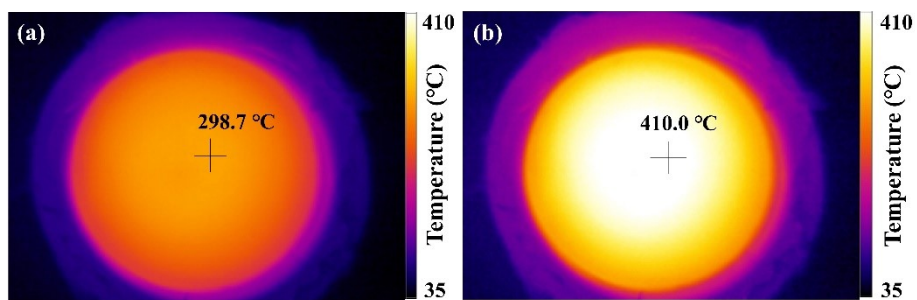


**Figure S20.** The IR images of the solar heating device under (a) 0.4 and (b) 1 kW m<sup>-2</sup> irradiation.

**Table S1.** The performance of representative catalysts for thermal catalytic FA decomposition.

Catalyst	Reaction condition	Temperature (°C)	Conversion (%)	H <sub>2</sub> selectivity (%)	H <sub>2</sub> generation rate (L g <sup>-1</sup> h <sup>-1</sup> )	Reference
<b>WN/Gr PF-850</b>	<b>FA</b>	<b>300</b>	<b>--</b>	<b>97.4</b>	<b>7.88</b>	<b>This work</b>
Mg <sub>1.0</sub> Mo <sub>99.0</sub> C <sub>1-x</sub>	FA	300	90+	90.0	--	1
α-Mo <sub>x</sub> C <sub>y</sub>	FA	300	100	89.0	--	2
1% Mo <sub>2</sub> C/Norit	FA	300	100	95.5	2.14	3
Mo <sub>2</sub> C/Gr	FA	380	37	86	--	4
MoS <sub>2</sub> /Mo <sub>2</sub> C	FA	220	97.4	99.2	--	5
10Mo <sub>x</sub> C/AC	FA	200	100	92	1.012	6
Mo <sub>2</sub> C-Co/GAC	FA	250	100	99.0	0.521	7
20% Mo-DAL	FA	220	98.0	99.4	--	5
PF-Mo <sub>1.98</sub> C <sub>1.02</sub>	FA/SF	100	--	97.6	0.79	8
γ-Mo <sub>2</sub> N/0.2NK-C	FA/H <sub>2</sub> O	87	100	100	0.2939	9
Ni <sub>10</sub> Mo <sub>1</sub> /PB	FA	300	92.8	98	--	10
Ni/G/MoS <sub>2</sub>	FA/SF	100	--	100	3.96	11
γ-Mo <sub>2</sub> N/NC	FA	200	100	99.4	1.84	12
Co@NC-Gr1	FA	300	100	~97	1.455	13
Ni <sub>0.40</sub> Au <sub>0.15</sub> Pd <sub>0.45</sub> /C	FA/H <sub>2</sub> O	25	73%	100%	--	14
Ag@Pd	FA/H <sub>2</sub> O	50	--	100%	5.60	15
Au <sub>0.03</sub> Pd <sub>0.05</sub> @BNNS	FA/NEt <sub>3</sub>	50		100%	1.26	16
2% Pd/ZnO	FA	287	100	~93%	1.63	17

Note: SF represents sodium formate; NEt<sub>3</sub> represents triethylamine.

**Table S2.** The performance of efficient photocatalysts for photocatalytic FA dehydrogenation.

Catalyst	Solvent	H <sub>2</sub> selectivity (%)	H <sub>2</sub> generation rate (L g <sup>-1</sup> h <sup>-1</sup> )	Reference
<b>WN/Gr PF-850</b>	<b>0.4 Sun</b>		<b>7.60</b>	<b>This work</b>
CdS/CoP@RGO	Xenon lamp	99.5%	4.07± 0.27	18
FeP@CdS NRs	Xenon lamp	--	6.227	19
Au <sub>0.75</sub> Pd/TiO <sub>2</sub>	1 Sun	99.5%	0.396	20
Ru-CdS	Xenon lamp	--	0.12	21
Pd/C <sub>3</sub> N <sub>4</sub>	Xenon lamp	--	1.19	22
Co <sup>2+</sup> /CdS QDs	Xenon lamp	99.4%±1%	2.59±0.31	23
CoPSA-CdS NRs	Xenon lamp	--	2.30	24
Fe salen/CdS	Xenon lamp	--	3.36	25
CdS/P/MoS <sub>2</sub>	Xenon lamp	--	1.54	26
Pt/g-C <sub>3</sub> N <sub>4</sub>	0.7 Sun	--	0.04	27

## References

1. J. Wang, J. Cao, Y. Ma, X. Li, P. Xiaokaiti, X. Hao, T. Yu, A. Abudula and G. Guan, Decomposition of formic acid for hydrogen production over metal doped nanosheet-like  $\text{MoC}_{1-x}$  catalysts, *Energy Convers. Manag.*, 2017, **147**, 166-173.
2. J. Cao, J. Wang, Y. Ma, X. Li, P. Xiaokaiti, X. Hao, A. Abudula and G. Guan, Hydrogen production from formic acid over morphology-controllable molybdenum carbide catalysts, *J. Alloys Compd.*, 2018, **735**, 1463-1471.
3. Á. Koós and F. Solymosi, Production of CO-free  $\text{H}_2$  by formic acid decomposition over  $\text{Mo}_2\text{C}$ /carbon catalysts, *Catal. Lett.*, 2010, **138**, 23-27.
4. J. Gray, S. Kang, J. Yang, N. Kruse, J. McEwen, J. Park and S. Ha, Unravelling the reaction mechanism of gas-phase formic acid decomposition on highly dispersed  $\text{Mo}_2\text{C}$  nanoparticles supported on graphene flakes, *Appl. Catal. B-Environ.*, 2020, **264**, 118478.
5. I. Kurnia, A. Yoshida, Y. Situmorang, Y. Kasai, A. Abudula and G. Guan, Utilization of dealkaline lignin as a source of sodium-promoted  $\text{MoS}_2/\text{Mo}_2\text{C}$  hybrid catalysts for hydrogen production from formic acid, *ACS Sustain. Chem. Eng.*, 2019, **7**, 8670-8677.
6. A. Carrales-Alvarado, A. Dongil, J. Fernández-Morales, M. Fernández-García, A. Guerrero-Ruiz and I. Rodríguez-Ramos, Selective hydrogen production from formic acid decomposition over Mo carbides supported on carbon materials, *Catal. Sci. Technol.*, 2020, **10**, 6790-6799.
7. S. Zhu, Z. Pan, Y. Tao and Y. Chen, Low temperature  $\text{H}_2$  production from formic



- acid aqueous solution catalyzed on metal doped Mo<sub>2</sub>C, *J. Renew. Mater.*, 2020, **8**, 939-946.
8. C. Lv, P. Lou, C. Shi, R. Wang, Y. Fu, L. Gao, S. Wang, Y. Li and C. Zhang, Efficient hydrogen production via sunlight-driven thermal formic acid decomposition over a porous film of molybdenum carbide, *J. Mater. Chem. A*, 2021, **9**, 22481-22488.
  9. Z. Yu, Y. Yang, S. Yang, J. Zheng, X. Hao, G. Wei, H. Bai, A. Abudula and G. Guan, Selective dehydrogenation of aqueous formic acid over multifunctional  $\gamma$ -Mo<sub>2</sub>N catalysts at a temperature lower than 100 °C, *Appl. Catal. B-Environ.*, 2022, **313**, 121445.
  10. L. Zheng, Z. Li, P. Fu, F. Sun, M. Liu, T. Guo and Q. Fan, Development of Mo-modified pseudoboehmite supported Ni catalysts for efficient hydrogen production from formic acid, *ACS Omega*, 2022, **7**, 27172-27184.
  11. X. Bai, S. Li, Y. Zhang, S. Zhu, L. Gao, R. Cong, W. Yu, S. Wang, B. Liang and Y. Li, Solar-heating thermocatalytic H<sub>2</sub> production from formic acid by a MoS<sub>2</sub>-graphene-nickel foam composite, *Green Chem.*, 2021, 7630-7634.
  12. Z. Yu, X. An, I. Kurnia, A. Yoshida, Y. Yang, X. Hao, A. Abudula, Y. Fang and G. Guan, Full spectrum decomposition of formic acid over  $\gamma$ -Mo<sub>2</sub>N-based catalysts: from dehydration to dehydrogenation, *ACS Catal.*, 2020, **10**, 5353-5361.
  13. A. Chernov, T. Astrakova, V. Sobolev and K. Koltunov, Liquid versus gas phase dehydrogenation of formic acid over Co@N-doped carbon materials. The role of single atomic sites, *Mol. Catal.* , 2021, **504**, 111457.

14. Z. Wang, Y. Ping, J. Yan, H. Wang and Q. Jiang, Hydrogen generation from formic acid decomposition at room temperature using a NiAuPd alloy nanocatalyst, *Int. J. Hydrog. Energy*, 2014, **39**, 4850-4856.
15. K. Tedsree, T. Li, S. Jones, C. Chan, K. M. Yu, P. Bagot, E. Marquis, G. Smith and S. Tsang, Hydrogen production from formic acid decomposition at room temperature using a Ag-Pd core-shell nanocatalyst, *Nat. Nanotechnol.*, 2011, **6**, 302-307.
16. S. Shaybanizadeh, A. Najafi Chermahini and R. Luque, Boron nitride nanosheets supported highly homogeneous bimetallic AuPd alloy nanoparticles catalyst for hydrogen production from formic acid, *Nanotechnology*, 2022, **33**, 275601.
17. D. Bulushev, M. Zacharska, S. Beloshapkin, Y. Guo and I. Yuranov, Catalytic properties of PdZn/ZnO in formic acid decomposition for hydrogen production, *Appl Catal A-Gen.*, 2018, **561**, 96-103.
18. S. Cao, Y. Chen, H. Wang, J. Chen, X. Shi, H. Li, P. Cheng, X. Liu, M. Liu and L. Piao, Ultrasmall CoP nanoparticles as efficient cocatalysts for photocatalytic formic acid dehydrogenation, *Joule*, 2018, **2**, 549-557.
19. T. Wang, L. Yang, D. Jiang, H. Cao, A. Minja and P. Du, CdS nanorods anchored with crystalline FeP nanoparticles for efficient photocatalytic formic acid dehydrogenation, *ACS Appl. Mater. Interfaces*, 2021, **13**, 23751-23759.
20. Z. Zhang, S. Cao, Y. Liao and C. Xue, Selective photocatalytic decomposition of formic acid over AuPd nanoparticle-decorated TiO<sub>2</sub> nanofibers toward high-yield hydrogen production, *Appl. Catal. B-Environ.*, 2015, **162**, 204-209.

21. Y. Zhang, L. Zhang and S. Li, Synthesis of Al-substituted mesoporous silica coupled with CdS nanoparticles for photocatalytic generation of hydrogen, *Int. J. Hydrog. Energy*, 2010, **35**, 438-444.
22. Y. Cai, X. Li, Y. Zhang, X. Wei, K. Wang and J. Chen, Highly efficient dehydrogenation of formic acid over a palladium-nanoparticle-based mott-schottky photocatalyst, *Angew. Chem. Int. Ed.*, 2013, **52**, 11822-11825.
23. M. Kuehnel, D. Wakerley, K. Orchard and E. Reisner, Photocatalytic formic acid conversion on CdS nanocrystals with controllable selectivity for H<sub>2</sub> or CO, *Angew. Chem. Int. Ed.*, 2015, **54**, 9627-9631.
24. P. Zhou, Q. Zhang, Z. Xu, Q. Shang, L. Wang, Y. Chao, Y. Li, H. Chen, F. Lv, Q. Zhang, L. Gu and S. Guo, Atomically dispersed Co-P3 on CdS nanorods with electron-rich feature boosts photocatalysis, *Adv. Mater.*, 2019, **32**, 1904249.
25. R. Irfan, T. Wang, D. Jiang, Q. Yue, L. Zhang, H. Cao, Y. Pan and P. Du, Homogeneous molecular iron catalysts for direct photocatalytic conversion of formic acid to syngas (CO+H<sub>2</sub>), *Angew. Chem. Int. Ed.*, 2020, **59**, 14818-14824.
26. J. Liu, H. Huang, C. Ge, Z. Wang, X. Zhou and Y. Fang, Boosting CdS photocatalytic activity for hydrogen evolution in formic acid solution by P doping and MoS<sub>2</sub> photodeposition, *Nanomaterials*, 2022, **12**, 561.
27. J. Wang, X. Wang, L. Qiu, H. Wang, L. Duan, Z. Kang and J. Liu, Photocatalytic selective H<sub>2</sub> release from formic acid enabled by CO<sub>2</sub> captured carbon nitride, *Nanotechnology*, 2021, **32**, 275404.